J. Earth Syst. Sci. (2023)132 23
https://doi.org/10.1007/s12040-022-02034-5

Early detection of heavy rainfall events associated with the monsoon in Kerala, India using GPS derived ZTD and PWV estimates: A case study

M S Rose[1], P S Sunil[1,*], Johnson Zacharia[2], K M Sreejith[3], S Sunda[4], V K Mini[5], A S Sunil[1] and K Vijay Kumar[6]

[1]*Department of Marine Geology and Geophysics, School of Marine Sciences, Cochin University of Science and Technology, Kochi, India.*
[2]*Tropical Marine Science Institute, National University of Singapore, Singapore, Singapore.*
[3]*Geosciences Division, Space Applications Centre, Ahmedabad, India.*
[4]*Airport Authority of India, Ahmedabad, India.*
[5]*Meteorological Centre, India Meteorological Department, Thiruvananthapuram, India.*
[6]*Indian Institute of Geomagnetism, Mumbai, India.*
**Corresponding author. e-mail: sunilps@cusat.ac.in*

MS received 10 February 2022; revised 19 August 2022; accepted 26 August 2022

The Precipitable Water Vapour (PWV) content associated with heavy precipitations can be estimated using the temporal variation of the Global Positioning System (GPS) derived Zenith Total Delay (ZTD). The ZTD and PWV were calculated using continuously observed GPS data for nine months (1 April to 31 December of 2018) that include the August 2018 catastrophic rainfall events in the state of Kerala, which is the gateway to the Indian summer monsoon located at southwest coast of India. The results show a precursory increment of ZTD followed by a decreasing phase before 5:45 h to 6:45 h of each heavy precipitation event. Further, the analysis of Radiosonde-derived ZTD for the past 45 years from 1973–2018 and GPS-derived ZTD from 2012–2018 reveal that during the onset of southwest monsoon over Kerala, the majority of the ZTD values converges within the range 2.55–2.70 m. The study exhibits that the GPS-derived ZTD could be effectively used for the real-time/short-term early detection of heavy precipitation events and to aid info on the onset time of southwest Indian summer monsoon.

Keywords. Summer monsoon; heavy precipitation; Zenith Total Delay; Precipitable Water Vapour; Global Positioning System; Radiosonde.

1. Introduction

Cloud, fog, and precipitation formation are influenced by water vapour condensation, one of the most critical rainfall activity parameters (Manandhar *et al.* 2018). Heavy rainfall events pose a serious threat to many populated and urbanized areas around the world (Ashley *et al.* 2005; Wheater and Evans 2009). An accurate estimate of the frequency and distribution of these events can help policymakers and observers to design better surveillance systems. In order to protect lives and property, disaster management agencies must be able to predict and warn of heavy rainfall events in vulnerable areas. In recent years, state-of-the-art numerical weather prediction

Published online: 01 February 2023

(NWP) models have been used to predict extreme rainfall events at various spatial and temporal scales (Lynch 2008; Bauer *et al.* 2015; Ashrit *et al.* 2020). However, the forecasts will always be uncertain due to errors in the initial conditions and approximations in the NWP model formulations. As a result, any method that can directly predict or provide early warning signals of extreme events will be extremely valuable.

The GPS technique has been developed to provide users around the world with accurate, continuous, three-dimensional position and velocity information (Kaplan and Hegarty 2005). However, it has evolved into a promising tool to monitor crustal deformation (Larson and Agnew 1991; Reddy and Sunil 2008; Sreejith *et al.* 2018), earthquake seismology (Larson 2009; Sreejith *et al.* 2016), ionospheric seismology (Lognonné *et al.* 2006; Ram *et al.* 2017), glacier dynamics (Frezzotti *et al.* 1998; Sunil *et al.* 2007), early tsunami warning (Blewitt *et al.* 2006; Bagiya *et al.* 2017), sea-level change (Löfgren and Haas 2014; Hammond *et al.* 2021), groundwater monitoring (Fu *et al.* 2012; Saji *et al.* 2020); growing vegetation (Small *et al.* 2010), soil moisture content (Larson *et al.* 2008), atmospheric water vapour content (Bevis *et al.* 1992, 1994; Jin *et al.* 2007; Jade and Vijayan 2008; Akilan *et al.* 2017; Zhao *et al.* 2018a, b), and other phenomena since the 1990s. A good example of an indirect solution for quantifying atmospheric humidity is the use of GPS tropospheric-induced signal delay to estimate PWV. Several earlier reports have established this relationship of GPS delay estimates with PWV as well as its efficiency in the estimation and forecasting of rainfall, particularly intense recipitation and weather dynamics (Suparta *et al.* 2012; Jiang *et al.* 2017; Sapucci *et al.* 2019). Furthermore, it is well established that GPS-derived Precipitable Water Vapour (hereafter referred to as GPS-PWV) is a promising tool for improving existing weather prediction systems (Cao *et al.* 2016; Zhao *et al.* 2018a, b). High moisture content, vertical movement, and static instability are all associated with heavy rainfall (Maddox 1979; Doswell *et al.* 1996). For well over a decade, researchers have been studying the relationship between deep convective activity, the occurrence of intense rainfall, and the temporal evolution of GPS-PWV. Wang *et al.* (2015) concluded that rapid increases in GPS-PWV in long-term low-level data predicted the arrival of rainfall and were thus useful in weather forecasting. Cao *et al.* (2016) reported that GPS-PWV could be used to improve near real-time/short-term rainfall forecasting. Shi *et al.* (2015) forecasted rainfall using an empirical real-time GPS-PWV threshold. However, Zhao *et al.* (2018b) have studied the feasibility of using GPS-derived Zenith Total Delay (hereafter referred to as GPS-ZTD) instead of GPS-PWV and shown that GPS-ZTD can be used for nowcasting of precipitation events.

The state of Kerala located on the southwest coast of India, popularly known as the gateway of the southwest Indian summer monsoon (Joseph *et al.* 1994), has a complex topography with the Arabian Sea to the west, ecologically fragile Western Ghats (also known as the Sahyadri) to the east and Indian Ocean to the south (figure 1). Physiographically, Kerala is divided into three zones: highland (>75.0 m), midland (7.5–75.0 m), and coastal plain (7.0 m) (Soman 1987). Kerala has an equable climate that fluctuates little from season to season due to its proximity to the sea and the existence of forts like the Western Ghats. Temperatures range between 27° and 32°C. The primary wet seasons are the southwest monsoon and the retreating monsoon (northeast monsoon). During the monsoon season, it receives a lot of rain, with an average of about 300 cm (Hunt and Menon 2020). In 2018, heavy rains from 7 to 17 August caused disastrous floods in many parts of the state, killing around 445 people and displacing 5.4 million others (UNDP 2018). India Meteorological Department (IMD) reported that the actual rainfall in Kerala from June to August 2018 was 15, 18, and 164% above the normal rate of precipitation, making the event the fourth-highest rainfall on record (MoES Report 2018). Kerala has over 43 dams and reservoirs that provide water for agriculture and hydropower generation (Ramasamy *et al.* 2019). Sporadic bouts of heavy rain (for example, 177.5 mm on August 17, 2018 in Idukki) in the Western Ghats' catchments prompted the reservoirs to reach full reservoir level (FRL), causing a surplus amount of water to be released through flood gates and it has intensified the number of casualties allied to the heavy precipitation (Duncombe 2018).

In this study, first, we have analyzed the feasibility of using GPS-ZTD in detecting heavy rainfall events rather than GPS-PWV. Further, by investigating the properties of GPS-ZTD, GPS-PWV, and Radiosonde-derived PWV (hereafter referred to as RAD-PWV), we conduct a case study related to the 2018 heavy rainfall events in Kerala.

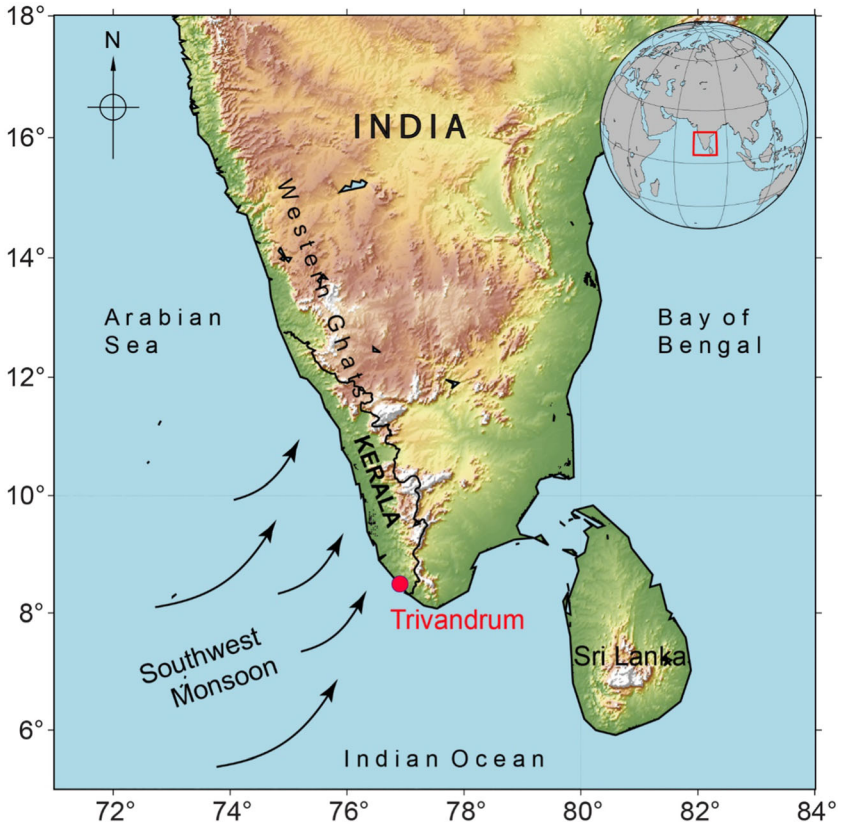

Figure 1. Map shows the GPS, Radiosonde and Meteorological observations site at Trivandrum in red circle. Arrows indicate the direction of southwest Monsoon.

Additionally, we carried out an analysis to estimate the characterization of GPS-ZTD and Radiosonde-derived ZTD (hereafter referred to as RAD-ZTD) from 1973 to 2018 during southwest monsoon onset time.

2. Data and methodology

This study primarily makes use of the continuous GPS data collected for the period of 1 April to 31 December 2018, which includes the August 2018 devastating rainfall events, at the Trivandrum Airport's GPS receiver site located 8.89°N, 76.90°E. In addition, the analysis of Radiosonde data for the past 45 years from 1973 to 2018 and GPS data from 2012 to 2018 from the same location is used to estimate the onset of southwest monsoon over Kerala.

The GPS site at Trivandrum has been established as part of the GPS-Aided GEO Augmented Navigation (GAGAN) network jointly implemented by the Indian Space Research Organization (ISRO) and the Airport Authority of India (AAI). The GPS data has been processed using the Canadian Spatial Reference System Precise Point Positioning (CSRS-PPP service version-2) by Natural Resources Canada (NRCan 2020). The Radiosonde observations (vertical resolution 30–100 m), which were launched twice a day at a 12-hr interval, were obtained from the University of Wyoming's upper air archive. The hourly rainfall data for the same period was obtained from the India Meteorological Department (IMD), Trivandrum, Kerala, rain gauge station located in the study region.

The GPS satellites' signal is delayed in time as it travels through the ionosphere and then the atmosphere. The induced dipole moment of the dry atmosphere (hydrostatic delay) and the permanent dipole moment of the water vapour (wet delay) both contribute to the atmospheric signal delay (Davis *et al.* 1985; Elgered 1993; Jade *et al.* 2005). At a specific location, the total tropospheric delay estimated by the GPS receiver from all satellites in different slant directions can be mapped into vertical using mapping functions to get the ZTD (figure 2). About 90% of the ZTD is contributed by

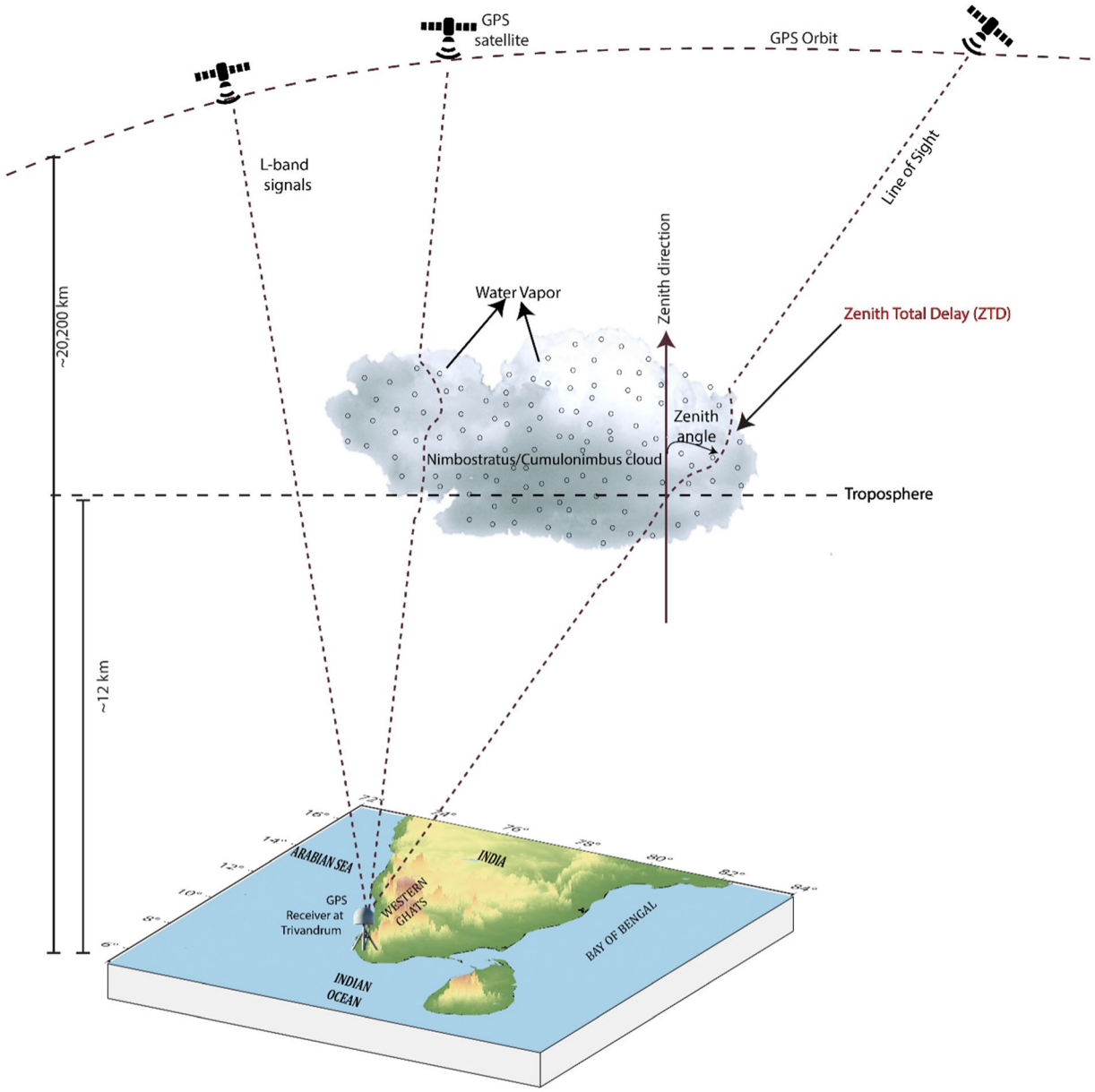

Figure 2. Schematic diagram depicts the GPS signal delay due to the presence of water vapour at any location using GPS-ZTD. In the present study, the observation site is at Trivandrum.

hydrostatic components and is termed as Zenith Hydrostatic Delay (ZHD), whereas the atmospheric water vapour contributes to the Zenith Wet Delay (ZWD), which accounts for less than 10% of total delay, i.e.,

$$\mathrm{ZTD} = \mathrm{ZHD} + \mathrm{ZWD}. \tag{1}$$

Based on the Saastamoinen model, the ZHD above a location can be represented as a function of surface pressure at the station using Saastamoinen formulas (Saastamoinen 1973) as modified by Davis *et al.* (1985),

$$\mathrm{ZHD} = \frac{0.002277 P_{\mathrm{s}}}{1 - 0.00266\cos(2\varphi) - 0.00028H} \tag{2}$$

where P_{s} and H are the surface pressure (hPa) and geodetic height (km) at the station, respectively and φ is the latitude.

Thus, PWV in a column of atmosphere can be derived as follows:

$$\mathrm{PWV} = \pi \mathrm{ZWD} \tag{3}$$

(Bevis *et al.* 1994) π being a conversion factor given as:

$$\pi = \frac{10^6}{\left(k_2 + \frac{k_3}{T_m}\right) R_v \rho} \tag{4}$$

where $k_2 = 16.48$ K/hPa and $k_3 = (3.776 \pm 0.014) \times 10^5$ K^2/hPa are constants, $R_v = 461$ (J/kg/K) represents the ideal gas constants for water vapour, ρ is the density of the water vapour and T_m is the mean temperature of the atmospheric column. This mean temperature is estimated using an empirical formula constrained by a large set of Radiosonde or reanalysis data (Bevis *et al.* 1994). In the present study, T_m is estimated from the Radiosonde observations from eight locations over the Indian subcontinent following the empirical relation (Suresh Raju *et al.* 2007) given by,

$$T_m = (62.6 \pm 1.67) + (0.75 \pm 0.006)\, T_s \tag{5}$$

where T_s is the surface temperature.

In order to estimate the uncertainty involved while estimating the mean tropospheric temperature from surface data using equation (5), we have estimated the weighted mean temperature (T_m) from Radiosonde observations at the study location (8.89°N, 76.90°E) for the years 2017 and 2018 using the equation (Yanxiong *et al.* 2012) given by,

$$T_m = \frac{\sum \frac{e}{T}(h_{(i+1)} - h_i)}{\sum \frac{e}{T^2}(h_{(i+1)} - h_i)} \tag{6}$$

where h_i and $h_{(i+1)}$ denote the height of two sequential observations, e and T are the average of water vapour pressure and absolute temperature, respectively, in the layer defined by h_i and $h_{(i+1)}$.

Here the vapour pressure 'e' is determined using Tetens equation. It is estimated that the uncertainty ranges between −2 and +1.

The elevation cut-off angle was set to 7.5° and to project the slant path delay to the station zenith position, Vienna Mapping Function 1 (VMF1) was applied. The quality of ZTD depends upon the number of GPS satellites visibility. At any location, a minimum of four satellites are required to estimate the position accurately. As the number of satellites increases, the quality of the estimated ZTD will also increase. The ZTD estimated thus obtained was used to retrieve the PWV using equations (1–5).

Further, the GPS-PWV was validated against the real-time RAD-PWV observed at the same location. The PWV for the sounding profile is estimated by integrating the specific humidity (q) from the surface to the top of the atmosphere.

$$\text{PWV} = \frac{1}{\rho g} \int_0^{P_s} q(p)\, dp \tag{7}$$

where ρ is the density of water vapour, g is the acceleration due to gravity, P_s is the surface pressure and $q(p)$ is the specific humidity at a pressure level p.

3. Results and discussions

3.1 *GPS-PWV and RAD-PWV*

The hourly GPS data for the period April to December 2018 is processed and analyzed along with the meteorological parameters (surface pressure and surface temperature) to derive ZTD, ZHD, ZWD, and PWV following the equations mentioned in section 2. Figure 3 shows the temporal variations of surface pressure, surface temperature, ZTD, ZWD, ZHD, and PWV during the period between 1 April and 31 December 2018. From the figure, it can be observed that ZTD, ZWD, and eventually, the PWV follow the same trend. However, the Zenith Hydrostatic Delay (ZHD), which accounts for about 90% of the ZTD varies slowly compared to the Zenith Wet Delay (ZWD). Moreover, the ZTD time series is characterized by troughs and crests, which indicates the corresponding variation of water vapour content in the atmosphere. The hourly ZTD ranges from 2.45 m towards the end of December (beginning of winter) to 2.5 m in pre-monsoon (April–May) and reaches a maximum of about 2.72 m during the southwest monsoon (June–September) and northeast monsoon (October–December). Whereas the GPS-PWV varies from 10 mm in winter to 75 mm during the summer monsoon season. To verify the reliability of GPS-PWV, it is validated with RAD-PWV for the period (1 April–31 December 2018 UTC 00:00 and 12:00 (daily)) utilizing the meteorological parameters estimated from the meteorological ground observatory at the location using equation (7). The RAD-PWV thus obtained at the Trivandrum site is compared with the GPS-PWV. The estimated GPS-PWV and RAD-PWV time series have a similar trend (figure 4) and are well associated with a correlation coefficient of 0.872 for the period (figure 5). However, there is a difference between RAD-PWV and GPS-derived PWV. It may be noted that, during the dry atmospheric condition, the presence of water

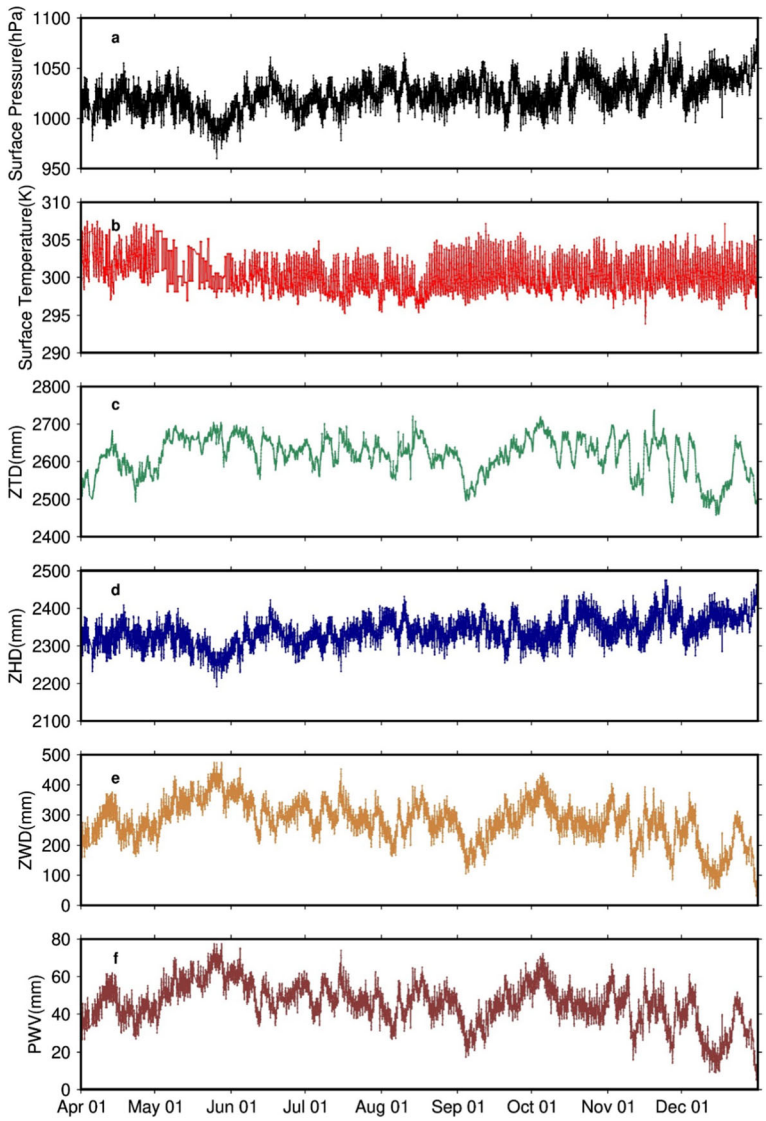

Figure 3. Hourly time series of (**a**) surface pressure, (**b**) surface temperature, (**c**) GPS-ZTD, (**d**) GPS-ZHD, (**e**) GPS-ZWD and (**f**) GPS-PWV for the period 1 April to 31 December of 2018 at Trivandrum location.

vapour in the atmospheric column is comparatively less than that of humid conditions. As a result, the wet delay induced by water vapour is also less, which in turn fluctuates the value of estimated PWV using GPS data.

3.2 *Relationship between ZTD and heavy rainfall events*

The association of GPS-PWV with severe weather events have been carried out by many investigators (Bevis *et al.* 1992; Rocken *et al.* 1995; Seco *et al.* 2012; Ortiz de Galisteo *et al.* 2014). However, accurate retrieval of PWV from GPS observations is challenging in the absence of collocated meteorological sensors. Therefore, it would be more advantageous if PWV could be replaced with ZTD for weather forecasting applications as it could be directly estimated from GPS observations. It may be noted that GPS-ZTD and GPS-PWV have very similar temporal variations, as depicted in figure 3. Few studies have reported the feasibility of ZTD instead of GPS-PWV as well. For example, Zhao *et al.* (2018b) have studied the feasibility of using ZTD instead of PWV and shown that GPS-ZTD can be used for nowcasting precipitation events. Giannaros *et al.* (2020) emphasized the positive impact of ZTD assimilation on the model's ability to forecast precipitation.

To delineate the behaviour of GPS-ZTD retrievals during intense rainfall events, the comparison of ZTD and hourly rainfall time series at Trivandrum for the period of 1 April to 31

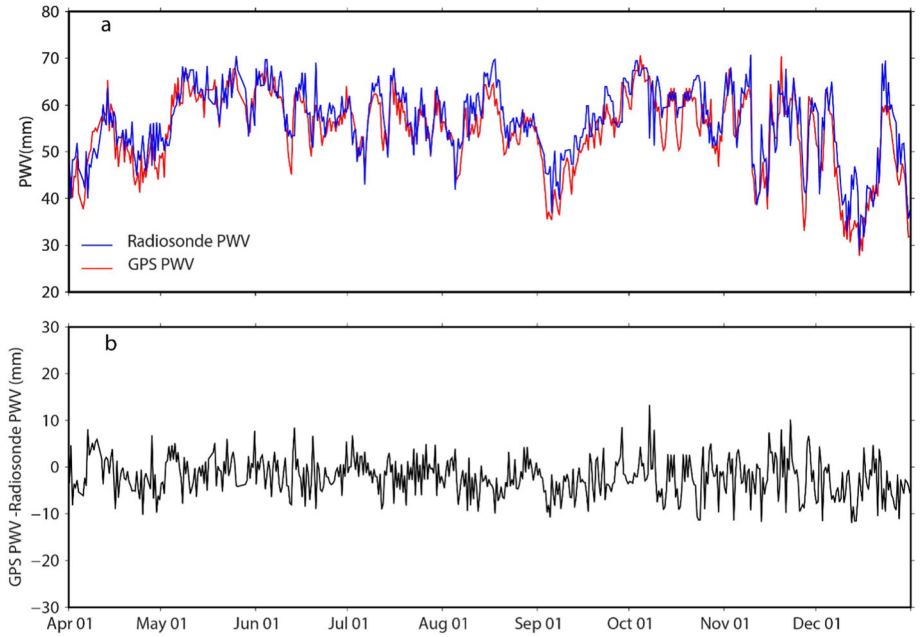

Figure 4. (**a**) Time series of GPS-PWV (shown in red) and RAD-PWV (shown in blue) for the period 1 April to 31 December of 2018 at Trivandrum location. (**b**) Exhibits the difference between GPS-PWV and RAD-PWV.

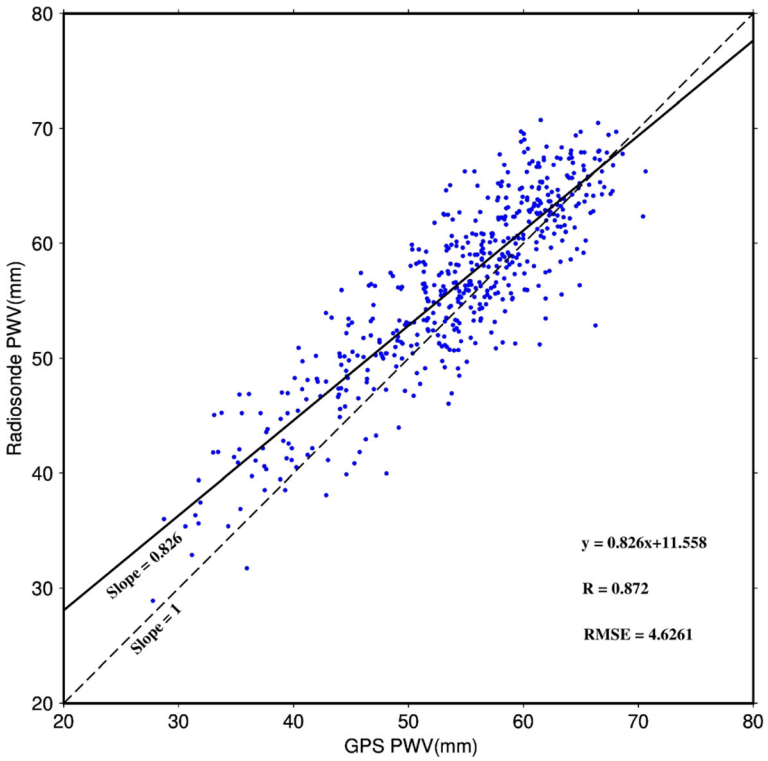

Figure 5. Correlation between GPS-PWV (mm) and RAD-PWV (mm). The dashed line shows the best fit curve with a correlation coefficient (R) of 0.872.

December 2018 were used (figure 6). The ZTD sampled at 10-second intervals corresponding to 10 events were chosen to analyze the ZTD variation associated with the rainfall events. The events of maximum rainfall corresponding to pre-monsoon, co-monsoon (southwest monsoon), and post-monsoon (northeast monsoon), and winter seasons were categorically chosen in order to verify the efficiency of ZTD during all the weather conditions.

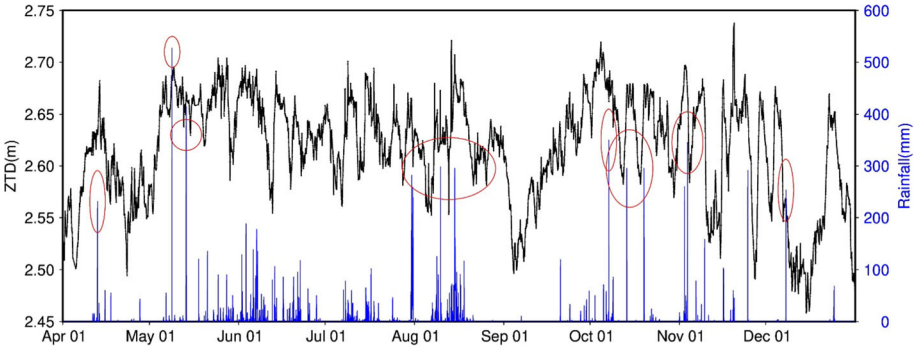

Figure 6. Time series of rainfall (mm) superimposed over GPS-ZTD (m) at the study location for the period 1 April to 31 December 2018. Heavy rainfall events and corresponding ZTD are marked within circles.

To understand the relationships between GPS-ZTD and heavy rainfall events in detail, these 10 heavy rainfall events are illustrated distinctly in figure 7(a–j). It is clearly evident that there is a steady increase in ZTD before each precipitation event, and precipitation occurs when the ZTD reached its peak value. The ZTD value returned to its stable value after precipitation, implying an atmospheric advection process as suggested by Zhao *et al.* (2018b). The peaks in ZTD are observed from 5:45 to 6:45 hours prior to precipitation (figure 7) and the ZTD values associated with the heavy rainfall events range from 2.65 to 2.75 m (figure 8). Although there are numerous peaks and troughs connected to the events, in most cases, the larger peaks of ZTD are associated with heavy precipitations. We have verified quite a number of observations and in the majority cases the precipitation peak occurred during the declining stage of ZTD from its peak value, approximately after 6 hrs. It may be noted that we are not making a one-to-one correlation between the intensity of ZTD and precipitation, rather an observation that the precipitation peak occurs during the declining stage of ZTD after the occurrence of its maximum value. There are several factors that influence precipitation. Akilan *et al.* (2015) have observed that the accumulated water vapour precipitates as rain at the same location under normal conditions. But the influence of atmospheric winds can take this water vapour to distant places and may precipitate there under suitable circumstances. As a result, not all the ZTD peaks are followed by same amount of precipitation.

Compared to all three monsoon periods (i.e., pre-monsoon, monsoon, and post-monsoon), pre-monsoon and southwest monsoon seasons (figure 7a–e) are distinguished by higher ZTD values than the northeast monsoon (figure 7f–j). It may be noted that higher values of ZTD can be indicative of the saturated atmospheric conditions during the pre- and co-monsoon periods (Fujita and Sato 2017). Unlike the southwest monsoon events, the rate of increase and decrease of ZTD is slow in northeast monsoon events. However, the ZTD peaks of the northeast monsoon events (figure 7f–j) are associated with thunderstorms and lightning activities during the post-monsoon season (Manohar and Kesarkar 2005).

As seen in figure 7(a–j), the evolution of ZTD follows a predictable pattern in circumstances of considerable precipitation, which may aid forecasting. Because precipitation requires a sufficient supply of water vapour, ZTD variations increase gradually before precipitation, resulting in a continuous increase in the amount of water vapour in the atmosphere in few hours, or even more than that, before precipitation, increasing the amount of ZTD and encapsulating the growing trend of ZTD (Zhao *et al.* 2018a). It should be noted that ZTD changes are not smooth, and some minor fluctuations are induced by external dynamic causes; however, the overall trend of ZTD increasing before precipitation and decreasing after precipitation is confirmed.

Similar types of observations were reported by Kursinski *et al.* (2008) and Shi *et al.* (2015) in the correlation of GPS-PWV and precipitation. Kursinski *et al.* (2008) observed that the precipitation is followed by a well-defined sharp increase in the GPS-PWV time series. Shi *et al.* (2015) proposed that an ascending and descending pattern of GPS-PWV is observed around each precipitation event.

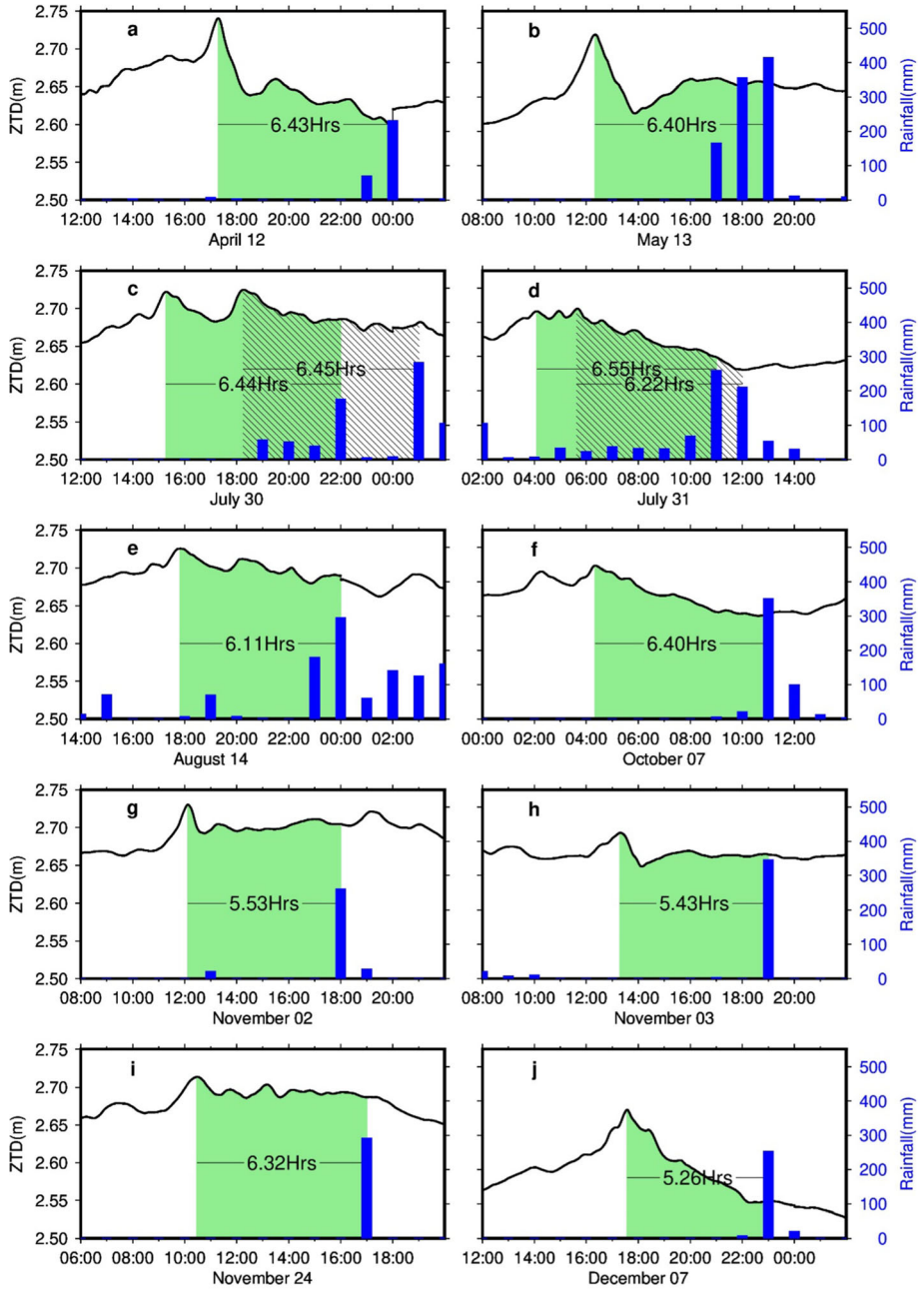

Figure 7. Relationship between selected heavy rainfall events and GPS-ZTD during pre-monsoon (**a**, **b**), southwest monsoon (**c–e**), and northeast monsoon (**f–j**) period for the year 2018 at Trivandrum. The black lines and blue bars indicate the ZTD and precipitation respectively. The green and grey line shadings represents the time interval between ZTD peaks and precipitation for each events. X-axis represents the time in UTC.

3.3 *GPS-derived ZTD during flash flood events*

Kerala, a small state in the southwestern Indian peninsula with an area of 38,863 km^2 (figure 1), receives monsoon rain and thundershowers for approximately 6 months of the year. However, during June 1 and August 29, 2018, the State has received 36% more rainfall than typical, resulting in extensive floods, landslides, around 445 deaths and the fourth-highest rainfall on record. In order to verify the behavior of the GPS-ZTD during severe flash flood events, we have chosen two extreme rainfall events based on the occurrence of maximum precipitation that happened in Trivandrum, Kerala, in August 2018. The first event occurred between August 7 and 10, and the second occurred between August 12 and 19 and was characterized by continuous downpours. To investigate further, we have analyzed *in-situ* meteorological parameters from the location

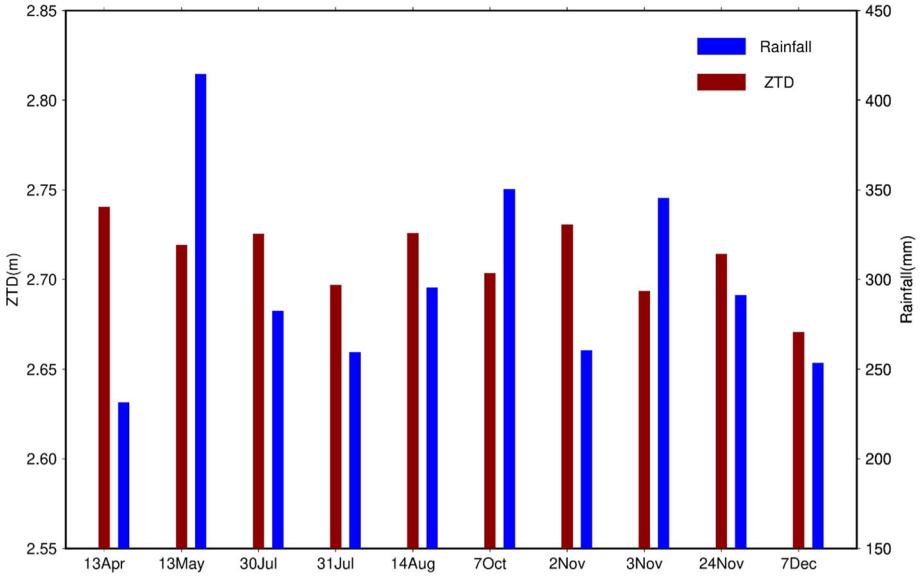

Figure 8. The ZTD maximum (brown bars) distribution corresponding to the precipitation events (blue bars) selected for analysis.

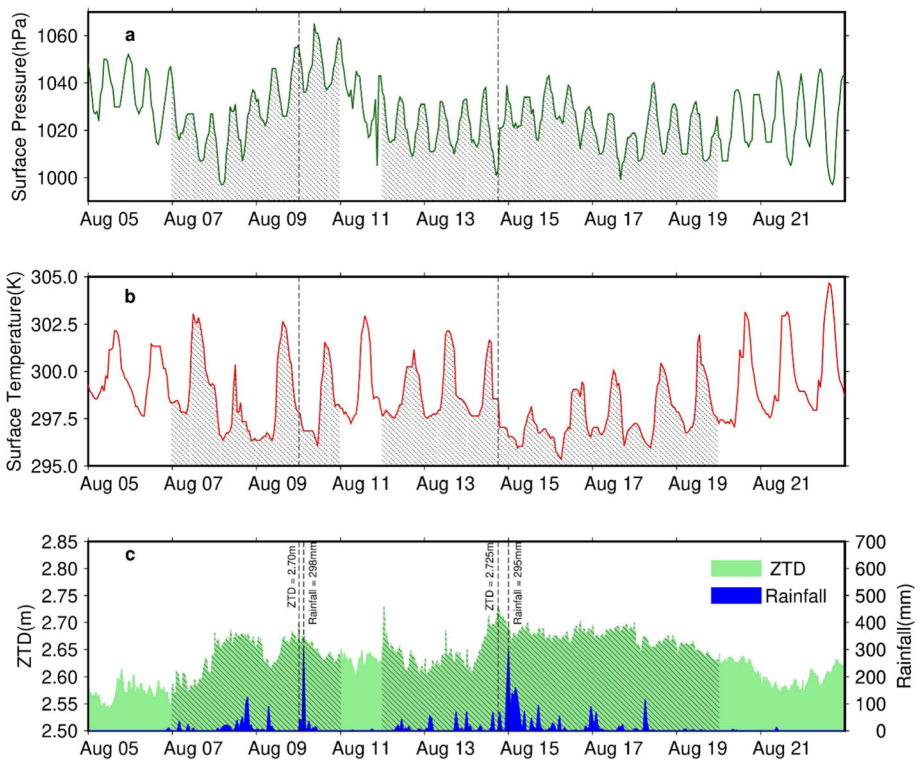

Figure 9. Time-series of (**a**) surface pressure (hPa), (**b**) surface temperature (K) and (**c**) rainfall (mm) superimposed over ZTD (m) during the period between 2018 August 5 and August 21 at Trivandrum. The vertical dashed line indicates the peaks in rainfall (blue) and corresponding ZTD, pressure, and temperature (green) values. The shade region shows the heavy precipitation days during August 7–10 and August 12–19.

Trivandrum (figure 1). Figure 9 represents the surface pressure, surface temperature, and rainfall superimposed over ZTD during the period from 7 to 19 August, 2018 at this location. The ZTD values shown in figure 9(c) are derived using surface pressure and surface temperature measurements from this location following equations (1–5). From figure 9, it can be observed that the ZTD increments observed on days August 7, 11, and 15 are associated with lower pressure values compared to

those observed on other days. It is also evident that during the period between August 7 and 10, ZTD values increased from 2.5 to 2.7 m. It can also be observed that each precipitation recorded during this period is preceded by significant ZTD jumps, which are always associated with a decreasing phase. It is interesting to note that rainfall occurs during the decreasing phase of ZTD jump.

Likewise, during the second event between August 12 and 19, precipitation was preceded by a buildup of ZTD jump with a maximum of about 2.725 m at 18:00 hrs on August 14 (figure 9c). Throughout the days of continuous precipitation, the ZTD values range as well as maintain between 2.55 and 2.725 m which is an indication of a highly saturated atmosphere (Fujita and Sato 2017). According to Kumar *et al.* (2020), during the time of heavy precipitation in August 2018, which led to the flash flood, the specific humidity reached up to 350 mb over Kerala, while it was around 600 mb over the Bay of Bengal, and the middle troposphere was found to be wetter than the boundary layer, with strong upward flow leading to precipitations from August 14 to 16 in Kerala. Vijaykumar *et al.* (2021) reported that the 2018 flood event was linked to a mesoscale cloudburst and structural changes in monsoon clouds over India's west coast. Both findings, however, are in line with our ZTD results.

3.4 *Characterization of GPS-ZTD and RAD-ZTD during monsoon onset*

Over peninsular India, the southwest monsoon arrives first in Kerala, signalling the start of the rainy season on the Indian subcontinent. This is known as Monsoon onset over Kerala (MooK) (Slingo 1999). As a result, a strong cross-equatorial low-level jet forms and moves across the Somali coast into the near-equatorial Arabian Sea, bringing heavy rains to the southern peninsula (Ramage 1971; Rao 1976). Monsoon onset has an imprint over southern peninsular India with seasonal reversal of surface and upper atmospheric wind and surface convection associated with the built-up of temperature and pressure contrast between the Indian continent and the Indian Ocean during March–May (Pradhan *et al.* 2017).

The India Meteorological Department (IMD) used to issue the monsoon onset date over Kerala every year using a statistical model that includes six predictors: minimum temperature over northwest India; pre-monsoon rainfall over the south peninsula; Outgoing Long Wave Radiation (OLR) over the South China Sea; lower tropospheric zonal wind over southeast Indian ocean; and upper tropospheric zonal wind over the eastern equatorial region (IMD Press release 2020). Early or delayed monsoon onset can have serious consequences for agriculture and other planning activities in the country (Aijaz 2013). As a result, an accurate onset date forecast can greatly aid in mitigating the adverse impacts of early or delayed onset. However, the onset prediction is still an untamed beast. As a result, any method, minor or major, that provides some insight into the onset prediction will be an added advantage.

Deciphering the behaviour of ZTD associated with the onset of the monsoon will be beneficial in this context. The ZTD associated with onset for the years 1973–2018 was calculated in order to examine the characteristics of ZTD for these years to see if they follow any particular pattern in and around monsoon onset days. Due to the lack of GPS data for the location from 1973 to 2011, an empirical method was devised to backtrack the ZTD from 1973 to 2011. The empirical method is explained as follows. First, the PWV is estimated from the Radiosonde data available at the location

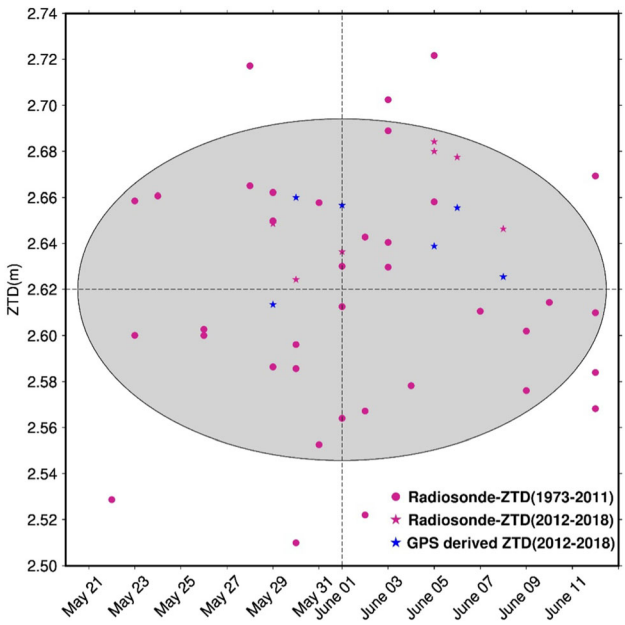

Figure 10. ZTD values corresponding to southwest monsoon onset days for the period from 1973 to 2018. The pink dots represent the ZTD values for the onset dates derived using Radiosonde data for the period 1973–2011. The blue and pink stars represent the ZTD values for the onset days derived from GPS and Radiosonde data for the period 2012–2018, respectively.

for the onset dates for the corresponding years during the period (1971–2011). This PWV is utilized to estimate ZWD using equation (3) mentioned in section 2. Then ZHD is calculated from equation (2) and using equation (1), ZTD is derived. From the scatter plot (figure 10), it is observed that the majority of the ZTD values corresponding to the monsoon onset days for the past 45 years (1973–2018) converge within the range 2.55–2.70 m and the inter-annual standard deviation of ZTD on the date of MooK is estimated to be 0.054 m. Thus, it can be expected, to an extent, that when ZTD values fall within the above-mentioned range during the pre-monsoon to monsoon transition time, it could be an indication of monsoon onset.

4. Conclusions

The reliability of GPS-PWV in detecting heavy rainfall events was investigated in this study. The estimated GPS-PWV and RAD-PWV for the period 1 April to 31 December 2018 have a correlation coefficient of 0.872, indicating that they are in good agreement with each other. Since GPS-ZTD estimation is easier and cost effective than GPS-PWV, the characteristics of the same over a spell were analyzed to understand feasibility to replace GPS-PWV with GPS-ZTD in meteorological applications. It is found that GPS-PWV and GPS-ZTD follow similar type of temporal variations. The analysis of the GPS-ZTD retrievals during intense rainfall events shows that ZTD peaks before the occurrence of a heavy rainfall event followed by a decreasing phase and the heavy rainfall occur 5:45–6:45 h after the ZTD peaks. During prolonged and heavy rainfall events, ZTD values typically range from 2.65 to 2.75 m, indicating a highly saturated atmosphere. In light of current analysis, the GPS-ZTD can be used as real-time/short-term advance monitoring of heavy rainfall events cost-effectively. An additional analysis of GPS-ZTD and RAD-ZTD associated with the onset of the southwest monsoon for the past 45 years (1973–2018) shows that during the pre-monsoon to monsoon transition onset time, the ZTD value ranges between 2.55 and 2.70 m and the inter-annual standard deviation of ZTD on the date of MooK is estimated to be 0.054 m. The present study is intended to test the feasibility of the ZTD estimates derived from GPS data for forecasting heavy precipitation events. However, in order to establish this technique, we recommend further analyses with many case studies in different climate conditions.

Acknowledgements

This work was carried out as part of the ISRO-SAC, NavIC-GAGAN, NGP-7 and DST-SERB, EEQ/2018/001480 sponsored projects in the Department of Marine Geology and Geophysics, Cochin University of Science and Technology, India. We thank the support received from the Cochin University of Science and Technology, Kochi and Indian Institute of Geomagnetism, Mumbai, for the initial approvals to carry out the work. The authors gratefully acknowledge the Airport Authority of India (AAI), Ahmedabad, and India Meteorological Department (IMD), Thiruvananthapuram, for providing GPS and Rainfall data, respectively. The figures were prepared by Generic Mapping Tools (GMT) (https://www.generic-mapping-tools.org/). The authors also thank both anonymous reviewers and Corresponding Editor for their constructive comments.

Author statement

MSR: Data analysis, interpretation, figure preparation and initial manuscript drafting. PSS: Conceptualization, supervision, interpretation and manuscript co-drafting. JZ: Discussion, interpretation and manuscript co-drafting. KMS: Discussion and critical review of the manuscript. SS: Discussion and provided GPS data. VKM: Discussion and provided rainfall data. ASS: Discussion and help in figure preparation. KVK: Discussion and manuscript review.

References

Aijaz R 2013 Monsoon variability and agricultural drought management in India; *Observer Research Foundation Issue Brief.* **51** 1–8.

Akilan A, Abdul Azeez K K, Balaji S, Schuh H and Srinivasa Y 2015 GPS derived zenith total delay (ZTD) observed at tropical locations in south India during atmospheric storms and depressions; *J. Atmos. Sol.-Terr. Phys.* **125** 1–7.

Akilan A, Balaji S, Abdul Azeez K K and Satyanarayanan M 2017 Source and causes of 2015 great pluvial flood of

Chennai, Tamil Nadu and its surroundings; *J. Geol. Soc. India* **90** 602–608.

Ashley R M, Balmforth D J, Saul A J and Blanskby J D 2005 Flooding in the future–predicting climate change, risks and responses in urban areas; *Water Sci. Technol.* **52(5)** 265–273.

Ashrit R, Sharma K and Kumar S 2020 Prediction of the August 2018 heavy rainfall events over Kerala with high-resolution NWP models; *Meteorol. Appl.* **27(e1906)**, https://doi.org/10.1002/met.1906.

Bagiya M S, Kherani E A, Sunil P S, Sunil A S, Sunda S and Ramesh D S 2017 Origin of the ahead of tsunami traveling ionospheric disturbances during Sumatra tsunami and offshore forecasting; *J. Geophys. Res.: Space Phys.* **122** 7742–7749, https://doi.org/10.1002/2017JA023971.

Bauer P, Thorpe A and Brunet G 2015 The quiet revolution of numerical weather prediction; *Nature* **525** 47–55, https://doi.org/10.1038/nature4956.

Bevis M, Businger S, Herring T A, Rocken C, Anthes R A and Ware R H 1992 GPS meteorology: Remote sensing of atmospheric water vapour using the global positioning system; *J. Geophys. Res.* **97(D14)** 787–801, https://doi.org/10.1029/92jd01517.

Bevis M, Businger S, Chiswell S S, Herring T A, Rocken C, Anthes R and Ware R H 1994 GPS Meteorology, Mapping zenith wet delays onto precipitable water; *J. Appl. Meteorol. Climatol.* **33** 379–386.

Blewitt G, Kreemer C, Hammond W C, Plag H P, Stein S and Okal E 2006 Rapid determination of earthquake magnitude using GPS for tsunami warning systems; *Geophys. Res. Lett.* **33** L11309, https://doi.org/10.1029/2006GL026145.

Cao Y J, Guo H, Liao R W and Uradzinski M 2016 Analysis of water vapour characteristics of regional rainfall around Poyang Lake using ground-based GPS observations; *Acta Geod. Geophys.* **51(3)** 467–479.

Davis J L, Herring T A, Shapiro I I, Rogers A E E and Elgered G 1985 Geodesy by radio interferometry: Effects of atmospheric modeling errors on estimates of baseline length; *Radio Sci.* **20(6)** 1593–1607, https://doi.org/10.1029/RS020i006p01593.

Doswell C A, Brooks H A and Maddox R A 1996 Flash flood forecasting: An ingredients-based methodology; *Wea. Forecasting* **22** 9811002.

Duncombe J 2018 Making sense of landslide danger after Kerala's floods; *Eos* **99**, https://doi.org/10.1029/2018EO108061.

Elgered G 1993 Tropospheric radio-path delay from ground-based microwave radiometry; *Atmospheric Remote Sensing by Microwave Radiometry,* Wiley & Sons Inc., pp. 218–258.

Frezzotti M, Capra A and Vittuari L 1998 Comparison between glacier ice velocities inferred from GPS and sequential satellite images; *Ann. Glaciol.* **27** 54–60.

Fu Y, Freymueller J T and Jensen T 2012 Seasonal hydrological loading in southern Alaska observed by GPS and GRACE; *Geophys. Res. Lett.* **39** L15310, https://doi.org/10.1029/2012GL052453.

Fujita M and Sato T 2017 Observed behaviors of precipitable water vapour and precipitation intensity in response to upper air profiles estimated from surface air temperature; *Sci. Rep.* **7** 4233, https://doi.org/10.1038/s41598-017-04443-9.

Giannaros C, Kotroni V, Lagouvardos K, Giannaros T M and Pikridas C 2020 Assessing the Impact of GNSS ZTD Data Assimilation into the WRF Modeling System during High-Impact Rainfall Events over Greece; *Remote Sens.* **12(3)** 383, https://doi.org/10.3390/rs12030383.

Hammond W C, Blewitt G, Kreemer C and Nerem R S 2021 GPS Imaging of global vertical land motion for studies of sea level rise; *J. Geophys. Res.: Solid Earth* **126**, https://doi.org/10.1029/2021JB022355.

Hunt K M R and Menon A 2020 The 2018 Kerala floods: A climate change perspective; *Clim. Dyn.* **54** 2433–2446, https://doi.org/10.1007/s00382-020-05123-7.

India Meteorological Department Press release, 15 May 2020, New Delhi.

Jade S and Vijayan M S M 2008 GPS-based atmospheric precipitable water vapour estimation using meteorological parameters interpolated from NCEP global reanalysis data; *J. Geophys. Res.: Atmos.* **113** D03106, https://doi.org/10.1029/2007JD008758.

Jiang W, Yuan P, Chen H, Cai J, Li Z, Chao N and Sneeuw N 2017 Annual variations of monsoon and drought detected by GPS: A case study in Yunnan, China; *Sci. Rep.* **7(1)** 1–10, https://doi.org/10.1038/s41598-017-06095-1.

Jin S, Park J U, Cho J H and Park P H 2007 Seasonal variability of GPS-derived zenith tropospheric delay (1994–2006) and climate implications; *J. Geophys. Res.* **112** D09110, https://doi.org/10.1029/2006JD007772.

Joseph P V, Eischeid J K and Pyle R J 1994 Interannual variability of the onset of Indian summer monsoon and its association with atmospheric features, El Nino and sea surface temperature anomalies; *J. Clim.* **7** 81–105.

Kaplan E and Hegarty C 2005 *Understanding GPS: Principles and applications*; Artech House, Norwood MA, 29p.

Kumar V, Pradhan P K, Sinha T, Rao S V B and Chang H P 2020 Interaction of a low-pressure system, an offshore trough, and mid-tropospheric dry air intrusion: The Kerala flood of August 2018; *Atmosphere* **11(7)**, https://doi.org/10.3390/atmos11070740.

Kursinski E R, Bennett R A, Gochis D, Gutman S I, Holub K L, Mastaler R, Minjarez Sosa C, Minjarez Sosa I and van Hove T 2008 Water vapour and surface observations in northwestern Mexico during the 2004 NAME enhanced the observing period; *Geophys. Res. Lett.* **35** L03815, https://doi.org/10.1029/2007GL031404.

Larson K M 2009 GPS Seismology; *J. Geodesy* **83** 227–233.

Larson K M and Agnew D C 1991 Application of the Global Positioning System to crustal deformation measurement. 1: Precision Accuracy; *J. Geophys. Res.* **96(B10)** 16,547–16,565.

Larson K M, Small E E and Gutmann E D 2008 Use of GPS receivers as a soil moisture network for water cycle studies; *Geophys. Res. Lett.* **35** L24405, https://doi.org/10.1029/2008GL036013.

Löfgren J S and Haas R 2014 Sea level measurements using multi-frequency GPS and GLONASS observations; *EURASIP J. Adv. Signal Process.* 50, https://doi.org/10.1186/1687-6180-2014-50.

Lognonné P, Garcia R and Crespon F 2006 Seismic waves in the ionosphere; *Europhys. News* **37(4)** 11–15, https://doi.org/10.1051/epn:2006401.

Lynch P 2008 The origins of computer weather prediction and climate modeling; *J. Comput. Phys.* **227(7)** 3431–3444, https://doi.org/10.1016/j.jcp.2007.02.034.

Maddox R A 1979 A methodology for forecasting heavy convective precipitation and flash flooding; *Nat. Weather Dig.* **4** 3042.

Manandhar S, Lee Y H, Meng Y S, Yuan F and Ong J T 2018 GPS-derived PWV for rainfall nowcasting in tropical region; *IEEE Trans. Geosci. Remote Sens.* **56** 4835–4844.

Manohar G K and Kesarkar A P 2005 Climatology and thunderstorm activity over Indian region: III. Latitudinal and seasonal variation; *Mausam* **56(3)** 581–592.

Ministry of Earth Sciences (MoES) 2018 Report on the exceptionally heavy rainfall over Kerala during 1st–19th Aug. 2018; https://sdma.kerala.gov.in/wp-content/uploads/2020/08/IMD-Monsoon-Extreme-Rainfall-2018.pdf.

NRCan 2020 Process global navigation satellite system data using the Canadian spatial reference system precise point positioning service – Natural Resources Canada; https://www.nrcan.gc.ca/maps-tools-and-publications/tools/geodetic-reference-systems/18766.

Ortiz de Galisteo J P, Bennouna Y, Toledano C, Cachorro V, Romero P, Andres M I and Torres B 2014 Analysis of the annual cycle of the precipitable water vapour over Spain from 10-year homogenized series of GPS data; *Quart. J. Roy. Meteorol. Soc.* **140(679)** 397–406.

Pradhan M, Rao A S, Srivastava A, Dakate A, Salunke K and Shameera K S 2017 Prediction of Indian summer-monsoon onset variability: A season in advance; *Sci. Rep.* **7(1)** 1–14, https://doi.org/10.1038/s41598-017-12594-y.

Ram S T, Sunil P S, Kumar M R, Su S Y, Tsai L C and Liu C H 2017 Coseismic traveling ionospheric disturbances during the Mw 7.8 Gorkha, Nepal, Earthquake on 25 April 2015 from ground and spaceborne observations; *J. Geophys. Res.: Space Phys.* **122** 10,669–10,685, https://doi.org/10.1002/2017JA023860.

Ramage C S 1971 Monsoon meteorology; *International Geophysics Series,* San Diego, CA: Academic Press, 296p.

Ramasamy S, Gunasekaran S, Rajagopal N, Saravanavel J and Kumanan C 2019 Flood 2018 and the status of reservoir-induced seismicity in Kerala, India; *Nat. Hazards* **99(4)** 1–13.

Rao Y P 1976 Southwest monsoon; *Meteorological Monograph* – Synoptic Meteorology, India Meteorological Department, New Delhi, No. 1/1976, 366.

Reddy C D and Sunil P S 2008 Post-seismic crustal deformation and strain rate in Bhuj region, western India, after the 2001 January 26 earthquake; *Geophys. J. Int.* **172** 593–606, https://doi.org/10.1111/j.1365-246X.2007.03641.x.

Rocken C, Hove T V, Johnson J, Solheim F, Ware R, Bevis M, Chiswell S and Businger S 1995 GPS/STORM – GPS sensing of atmospheric water vapour for meteorology; *J. Atmos. Ocean. Technol.* **12(3)** 468–478, https://doi.org/10.1175/1520-0426(1995)012.

Saastamoinen J 1973 Contributions to the theory of atmospheric refraction – Part II. Refraction corrections in satellite geodesy; *Bull. Géodésique* **47(1)** 13–34, https://doi.org/10.1007/BF02522083.

Saji A P, Sunil P S and Sreejith K M *et al.* 2020 Surface deformation and influence of hydrological mass over Himalaya and North India revealed from a decade of continuous GPS and GRACE observations; *J. Geophys. Res.: Earth Surf.* **125** e2018JF004943, https://doi.org/10.1029/2018JF004943.

Sapucci L F, Machado L A T, de Souza E M and Campos T B 2019 Global Positioning System precipitable water vapour (GPS-PWV) jumps before intense rain events: A potential application to nowcasting; *Meteorol. Appl.* **26(1)** 49–63, https://doi.org/10.1002/met.1735.

Seco A, Ramırez F, Serna E, Prieto E, Garcıa R, Moreno A, Cantera J C, Miqueleiz L and Priego E 2012 Rain pattern analysis and forecast model based on GPS estimated atmospheric water vapour content; *Atmos. Environ.* **49** 8593.

Shi J, Xu C, Guo J and Gao Y 2015 Real-time GPS precise point positioning-based precipitable water vapour estimation for rainfall monitoring and forecasting; *IEEE Trans. Geosci. Remote Sens.* **53(6)** 3452–3459, https://doi.org/10.1109/TGRS.2014.2377041.

Slingo J 1999 *The Indian summer monsoon and its variability beyond El Niño*; Springer, Berlin, Heidelberg, pp. 103–118, https://doi.org/10.1007/978-3-642-58369-8_5.

Small E E, Larson K M and Braun J J 2010 Sensing vegetation growth with reflected GPS signals; *Geophys. Res. Lett.* **37** L1201, https://doi.org/10.1029/2010GL042951.

Soman K 1987 *Geology of Kerala*, Geological Society of India, ISBN No: 81-85867-24-0.

Sreejith K M, Sunil P S, Agrawal R, Saji A P, Ramesh D S and Rajawat A S 2016 Coseismic and early post-seismic deformation due to the 25 April 2015, Mw 7.8 Gorkha, Nepal, earthquake from InSAR and GPS measurements; *Geophys. Res. Lett.* **43**, https://doi.org/10.1002/2016GL067907.

Sreejith K M, Sunil P S, Agrawal R, Saji A P, Ramesh D S and Rajawat A S 2018 Audit of stored strain energy and extent of future earthquake rupture in central Himalaya; *Sci. Rep.* **8** 1669, https://doi.org/10.1038/s41598-018-35025-y.

Sunil P S, Reddy C D, Ponraj M, Dhar A and Jayapaul D 2007 GPS determination of the velocity and strain-rate fields on Schirmacher Glacier, central Dronning Maud Land, Antartica; *J. Glaciol.* **53(183)** 558–564.

Suparta W, Adnan J and Ali M A M 2012 Monitoring of GPS precipitable water vapour during the severe flood in Kelantan; *Am. J. Appl. Sci.* **9(6)** 825–831, https://doi.org/10.3844/ajassp.2012.825.831.

Suresh Raju C, Saha K, Thampi B V and Parameswaran K 2007 Empirical model for mean temperature for Indian zone and estimation of precipitable water vapour from ground-based GPS measurements; *Ann. Geophys.* **25(9)** 1935–1948, https://doi.org/10.5194/angeo-25-1935-2007.

UNDP 2018 Kerala. Post-disaster needs assessments: Floods and landslides; https://www.undp.org/publications/post-disaster-needs-assessment-kerala.

Vijaykumar P, Abhilash S and Sreenath A V 2021 Kerala floods in consecutive years – Its association with mesoscale cloudburst and structural changes in monsoon clouds over the west coast of India; *Weather Clim. Extremes* **33**, https://doi.org/10.1016/j.wace.2021.100339.

Wang B Y, Zhao L N and Bai X M 2015 The characteristics investigation of ground-based GPS/PWV during the "7.21" extreme rainfall event in Beijing; *China Satellite Navigation Conference (CSNC) 2015 Proceedings*, pp. 563–574.

Wheater H and Evans E 2009 Land use, water management and future flood risk; *Land Use Policy* **26(1)** 251–264, https://doi.org/10.1016/j.landusepol.2009.08.019.

Yanxiong L, Chen Y and Liu 2001 Determination of weighted mean tropospheric temperature using ground meteorological measurements; *Geo. Spat. Inf. Sci.* **4(1)** 14–18, https://doi.org/10.1007/BF0282663026(1).

Zhao Q, Yao Y and Yao W 2018a GPS-based PWV for precipitation forecasting and its application to a typhoon event; *J. Atmos. Sol.-Terr. Phys.* **167** 124–133, https://doi.org/10.1016/j.jastp.2017.11.013.

Zhao Q, Yao Y, Yao W and Li Z 2018b Real-time precise point positioning-based zenith tropospheric delay for precipitation forecasting; *Sci. Rep.* **8(1)** 1–12, https://doi.org/10.1038/s41598-018-26299-3.

Corresponding editor: C Gnanaseelan